Laser and Particle Beams (2011), *29*, 39–44.

doi:10.1017/S026303461000073X

Inertial confinement fusion fast ignition with ultra-relativistic electron beams

C. DEUTSCH[1] AND J.-P. DIDELEZ[2]
[1]LPGP Universsité Paris-Sud (UMR-CNRS 8578), Orsay, France
[2]IPN, Université Paris-Sud (UMR-CNRS 8608), Orsay, France

(RECEIVED 15 October 2010; ACCEPTED 2 November 2010)

Abstract

Inertial confinement fusion fast ignition at very high relativistic electron beam energy is systematically explored through a possible combination of various stopping mechanisms including strong Langmuir turbulence, elastic, and inelastic electron interactions with target particles. A specific attention is given to final state interaction through catalysis by negative pion.

Keywords: ICF fast ignition; Pion catalysis; Relativistic electron beams; Very high energy

1. INTRODUCTION

In contradistinction to the main-stream fast ignition scenario (FIS), based on collisional stopping in the compressed deuterium tritium (DT)-fuel of relativistic electron beams (REB), in the 1–2 MeV energy range (ER) (Deutsch *et al.*, 1996, 1997), we consider an ultra relativistic extension of a previous attempt (Malkin & Fisch, 2002) by using REB in the several tenths of MeV ER, and stopping them in target through turbulence. Motivations for such an endeavor are obviously two-fold. First, conditions involving less initial intensity and easier "piercing" of the DT-precompressed core are electromagnetic instabilities. Moreover, the consideration of fast ignition guided with gold (Au) cone (Fig. 1) (Kodama *et al.*, 2002) opens an opportunity of producing hard X- and γ-rays in the cone, which altogether with REB can pave the way to producing many high energy nuclear reactions based on the exchange of virtual photons, i.e., nonhadronic.

We therefore stress the additional and substantial contribution to REB stopping of strongly inelastic reactions, such as the Trident production of electron-positron pairs. In the 100 MeV and higher ER bremsstrahlung turns significant and hard Gamma come also into play to enhance these processes. We thus specifically emphasize electro-disintegrating deuterons and tritons, first in nucleons and eventually at higher energy with negative pion production included. In the latter case, it seems attractive to considerer pion-catalyzed DT fusion in very dense and hot plasma with no sticking. This claim is supported by preliminary estimates based on Debye like diatomic plasma orbitals. More interplay between resulting positrons and pions of either sign are also seen to contribute to *in situ* stopping of ultra-relativistic REB. The latter would then drive efficiently a fast ignition target with significantly reduced beam intensity and no further hole boring issues.

Address correspondence and reprint requests to: C. Deutsch, LPGP Universsité Paris-Sud (UMR-CNRS 8578), Bât. 210, F-91405 Orsay, France. E-mail: Claude.deutsch@u-psud.fr

2. REB INTERACTION WITH INSTABILITIES

2.1. Electromagnetic Instabilities (EMI)

At moderate relativistic energy, i.e., for a Lorentz factor

$$\gamma_b = \frac{1}{\sqrt{1-\frac{v_b^2}{c^2}}} \leq 10$$

v_b denoting a monochromatic REB velocity, one is mostly concerned with beam propagation (Fig. 1) through electromagnetic instabilities (EMI) arising in the combined beam (density n_b)-target plasma (electron density n_p, plasma frequency ω_p). EMI are unfortunately able to spoil easily and degrade REB initial qualities through increased emittance, energy spread, beam break-up… Such a possibility is already quantified in the initial linear regime. Most significant EMI growth rates feature two-stream (TS), filamentation (F), and a TSF combination of both (Bret & Deutsch, 2005), for the dimensionless $Z_z = k_z V_p/\omega_p \sim 1$ with a maximum growth

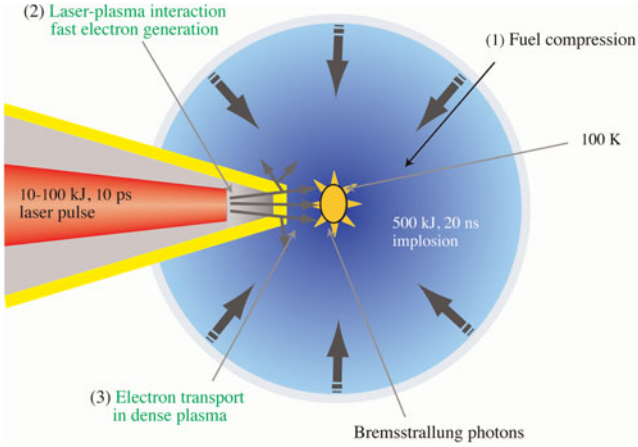

Fig. 1. (Color online) Cone-guided fast ignition with γ-production, through REB-Au interaction (after Kodama et al., 2002).

rate in ω_p units

$$\delta^{TS} \sim \frac{\sqrt{3}}{2^{4/3}} \frac{\alpha^{1/3}}{\gamma_b}, \alpha = \frac{n_b}{n_p}. \quad (1)$$

In the direction normal to the beam, the filamentation δ behaves for small $Z_x = k_x V_p/\omega_p$ as

$$\delta^{F} \sim \frac{\sqrt{\alpha}}{\gamma_b} Z_x, \quad (2)$$

and then saturates for $Z_x \gg V_b/c$ at

$$\delta^{F} \sim \sqrt{\frac{\alpha}{\gamma_b}}. \quad (3)$$

Absolute maximum growth rate for oblique wave vector is obtained with $Z_z \sim 1$ and $Z_x \gg 1$. We shall denote this maximum two-stream/filamentation growth rate as δ^{TSF} with

$$\delta^{TSF} \sim \sqrt{\frac{3}{2^{4/3}}} \left(\frac{\alpha}{\gamma_b}\right)^{1/3}. \quad (4)$$

As far as the hierarchy of these unstable modes is concerned, it is obvious that $\delta^{TSF} > \delta^{TS}$ for any sets of parameters, except in the non-relativistic regime $\gamma_b = 1$ where both growth rates are equal

2.2. Strong Langmuir Turbulence

On the other hand, at very high $\gamma_b \gg 1$ values, the nonlinear evolution of the EMI toward an electrostatic regime could induce an appropriate REB collective stopping in precompressed target (Malkin & Fisch, 2002). The latter is then monitored by $\theta = \text{angle}(\overrightarrow{REB},\vec{k})$ between initial REB direction and Langmuir (L) wave's number direction, while contrasting W_r, energy density in L waves resonating with REB to thermal energy density $W_{th} \sim n_p T_p^2/m_e c^2$ in target.

Local REB relaxation length in turbulence thus features

$$L_r \sim (c/2\omega_p)(m_e c^2/T_e)^2(\gamma_b \Delta\theta)^2(W_{th}/W_r).$$

For $\omega_p \sim 6 \times 10^{17}$ s^{-1} and $T_e \sim 5$ keV, this simplifies to

$$L_r \sim 2.5(\gamma_b \Delta\theta)^2(W_{th}/W_r)\mu m.$$

If $W_r > W_{th}$, this length would not exceed 50 μm for $\gamma_b \Delta\theta \leq 5$

2.3. EMHD

It has also been recently documented (Yabuuchi *et al.*, 2009) that electron magneto-hydrodynamic shock formation, i.e., with immobile ions, could stop high γ_b REB in the inhomogeneous density region (see Fig. 1). Such a mechanism seems to interpret the stopping of 15 MeV REB, in appropriate target with density $\rho \sim 50$–100 g/cm^3 recently observed experimentally at ILE (Osaka).

3. REB STOPPING ON TARGET ELECTRONS ($\gamma_B \gg 1$)

The stopping of uncorrelated and ultrarelativistic electron projectiles on target electrons taken as mostly classical ($T_p \geq 1$ keV) is accurately accounted for by a complete relativistic expression (Deutsch *et al.*, 1996, 2000) well approximated by a simple Bethelike one (Starikov & Deutsch, 2005) given as

$$-\frac{dE}{dx} = \frac{4\pi n e^4}{m v_b^2} \ln\left(\frac{2mc^2\gamma_b^2}{\hbar\omega_p}\right) = E n_p \sigma, \quad (5)$$

and also expressed in terms of an equivalent stopping cross-sections σ. For instance, at REB energy $E = 200$ MeV, one thus witnesses for $n_e \sim 10^{26}$ e-cm^{-3} (FIS conditions), $\sigma \sim 10^{-25}$ cm^2, a hundred times the Trident process for electroproduction of electron-position pairs on target ions. It is also of quantitative interest to notice that Eqs. (5) displays a slight logarithmic increase, V_b being fixed at c, above $E > 200$ MeV.

4. REB STOPPING ON TARGET IONS ($\gamma_b \gg 1$)

At ultra relativistic energy, the above elastic interaction with target electrons has to be supplemented by elastic interaction on target ions, which then exhibit their extended charge structure through electric and magnetic form factors (Hofstadter, 1963).

Elastic scattering of high-energy electrons by the magnetic moment of the proton had actually been predicted by Rosenbluth (1950), who showed that there is a contribution to the elastic scattering from both the Dirac and the Pauli components of the proton's magnetic moment. The Pauli

https://doi.org/10.1017/S026303461000073X Published online by Cambridge University Press

moment is usually referred to as the "anomalous" part of the proton's magnetic moment. These arguments may be rationalized as follows. For a protonic point charge with masse M and point magnetic moment (in nuclear magnetic n.m.), the differential cross section reads as

$$\left(\frac{d\sigma}{d\Omega}\right)_R = \left(\frac{e^2}{2E_b}\right)^2 \frac{\cos^2\theta/2}{\sin^4\theta/2} \frac{1}{1+\frac{2E_b}{Mc^2}} \sin^2\theta/2 \left\{1+\frac{\hbar^2 q^2}{4M^2c^2}\left[2(1+K)^2\tan^2\theta/2+K^2\right]\right\} \quad (6)$$

$(\mu_p = 1 + K = 2.79\text{n.m.}).$

in terms of momentum

$$q = \frac{2}{\lambda} - \left[1 + (2E_b/M)\sin^2\frac{1}{2}\theta\right]^{1/2}, \quad (7)$$

and reduced De Broglie wavelength

$$\lambda = \frac{\hbar}{p}, \text{ in C.M.S,}$$

of the electron projectile. θ denote the departure with respect to initial REB initial/direction. Eq. (6) is pictured in Figure 2 for several E_b values.

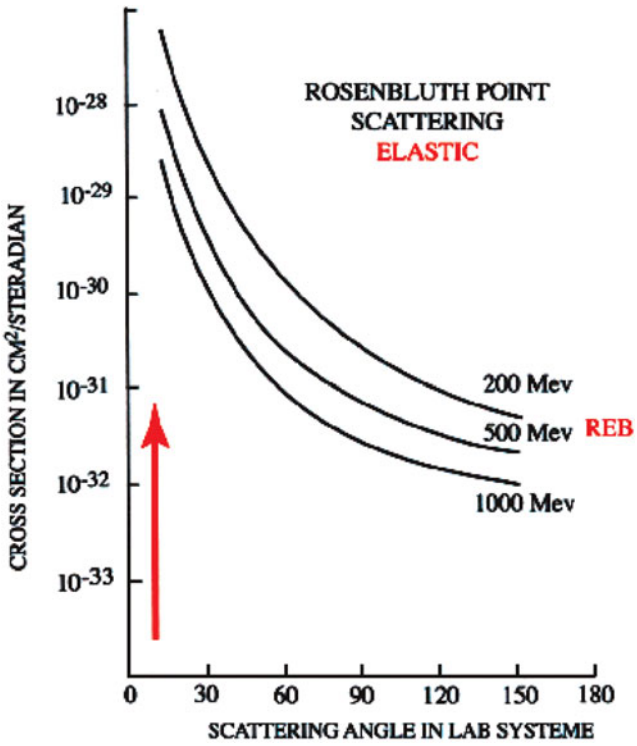

Fig. 2. (Color online) Rosenbluth-point scattering for point-protons with real values of nuclear spin and magnetic moment. The appropriate cross section is given with K = 1.79 nuclear magnetons, μ = 2.79 n.m. (after Hofstadter, 1963)

Switching to deuterium, Eq. (6) gets extended to

$$\left(\frac{d\sigma}{d\Omega}\right)_R = \sigma_{NS}\left\{1+\frac{2}{3}\frac{q^2}{4M_D^2}\left[2\mu_D^2\tan^2\frac{1}{2}\theta+\mu_D^2\right]\right\}F_D^2, \quad (8)$$

in terms of

$$\sigma_{NS} = \frac{e^4}{4E^2}\frac{\cos^2 1/2\theta}{\sin^4 1/2\theta}\frac{1}{1+(2E_b/M_D)\sin^2 1/2\theta},$$

M_D = deuteron mass

μ_D is the static deuteron magnetic moment, and F_D is the form factor obtainable from the deuteron's charge density, as determined from the wave function of the deuteron in its ground state. The second term in the bracket is the magnetic term. The spin of the deuteron is 1 and this accounts for the difference in the coefficient of the q^2 term between Eqs. (6) and (8).

In the case of breakup of the deuteron, involving inelastic scattering, for large moment transfers one gets (Hofstadter, 1963) the inelastic cross-section

$$\sigma_D^{in}(\theta) = \sigma_{NS}\left\{1 - F_D^2 + \frac{q^2}{4M2}\left[2(\mu_p^2+\mu_n^2-F_D^2)\tan^2 1/2\theta + \mu_p^2+\mu_n^2-3F_D^2\right]\right\}. \quad (9)$$

μ_p and μ_n are the proton and neutron magnetic moments, respectively, and F_D is the deuteron elastic form factor. When the momentum transfer is large, $F_D \cong 0$. Similar

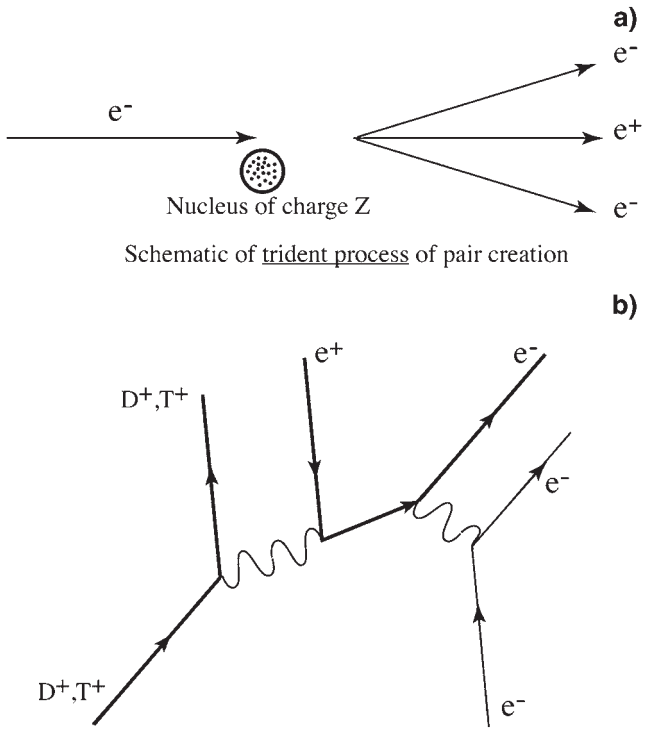

Fig. 3. (**a**) Trident process for pair production. (**b**) Trident Feynman graph for $e^+ + {}^{D^+}_{T^+} \rightarrow e^+ + e^- + {}^{D^+}_{T^+}$.

https://doi.org/10.1017/S026303461000073X Published online by Cambridge University Press

extensions may also be worked out for tritium. The above elastic expressions (Fig. 2) display a strong maximum in the forward ($\theta = 0$) direction. Corresponding integrated cross-sections then peak in the *mbarn* (10^{-27} cm^2) range.

5. ELECTRO- AND PHOTO-PRODUCTION OF ELECTRON-POSITRON PAIRS

At the equivalent *mb* level for the total cross-section, one also encounters the well-known Trident process (Figs. 3 and 4) (Shearer *et al.*, 1972) for the inelastic production of electron-position pairs on target ions with charge Z. This process gets even significantly enhanced when triggered out by γ rays produced in the cone area of the FIS target (Fig. 1). The given photons are then copiously produced in Au ($Z = 79$) through the ratio

$$\frac{\frac{dE}{dx_{rad}}}{\frac{dE}{dx_{coll}}} = E_b \frac{Z}{1600 m_e c^2}$$

reaching unity for $E = 10.35$ MeV in Au and $E = 817.16$ in DT that leads to the ratio (Myatt *et al.*, 2009)

$$\frac{\sigma_T}{\sigma_{\gamma\to e^+e^-}} = \frac{\alpha}{\pi}\left[\ln\left(\frac{E}{m_e c^2}\right)\ln\left(\frac{E}{2.137 m_e c^2 Z^{-1/3}}\right) + \frac{1}{3}\ln^2(2.137 Z^{-1/3})\right] = 0.017 \text{ at 5 MeV in Au,} \quad (10)$$

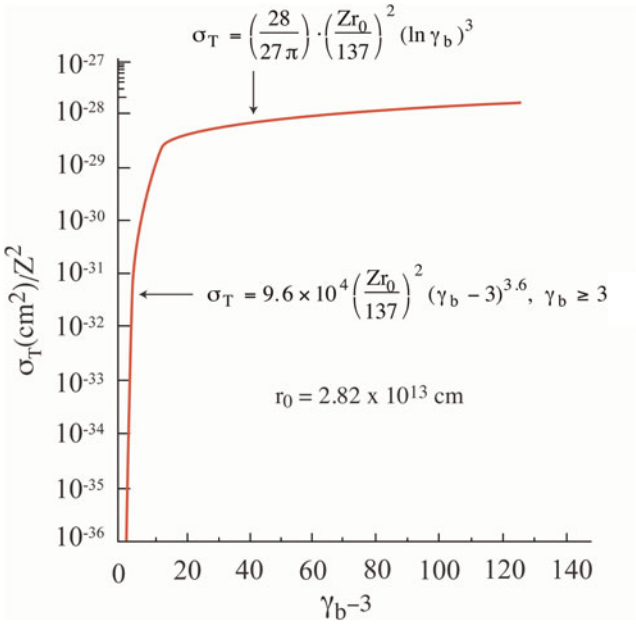

Fig. 4. (Color online) Total cross section σ_T of the Trident process plotted versus the dimensionless electron-energy excess above the threshold. Here $\gamma_b = E_b/m_e c^2$. Z denotes target ion nuclear charge.

where $\alpha = 1/137.036$ is the quantum electrodynamics fine structure constant.

6. NEGATIVE PION ELECTRO-PRODUCTION

Turning attention to the many channels available to nuclei electro-disintegration, we first focus on the basic Möller diagram (Fig. 5a) pictured à la Feynman with the exchange of one single virtual photon. Its robustness up to $E_b = 1$ GeV is highlighted by the very low level of requested radiative corrections, and the negligibility of multiple and virtual proton exchange. A preliminary disintegration stage involves proton out of deuterium, and deuterium out of tritium. However, as soon as $E_b \geq 145$ MeV, the channels of negative pion production open up (Figs. 5b, 5c). Pertaining totally

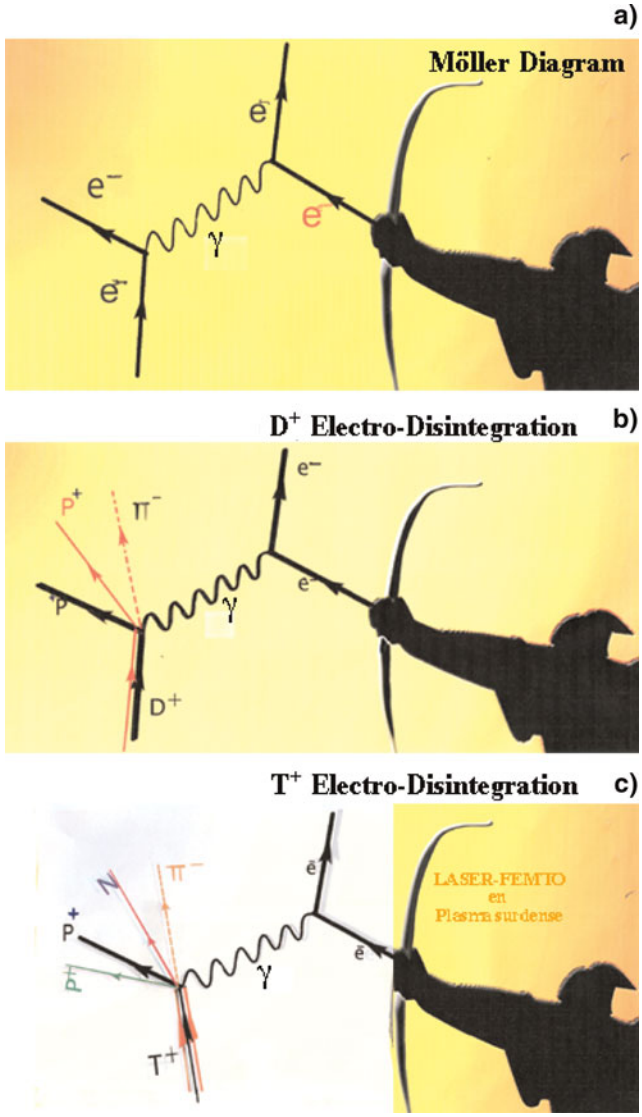

Fig. 5. (Color online) (**a**) Electron-electron covariant Möller diagram. (**b**) D-Electro-disintegration and (**c**) T- Electrodisintegration. In (b) and (c) π^- appears when $E_b \geq 150$ MeV. Robin Hood pictures a PW-laser (after N. Deutsch)

https://doi.org/10.1017/S026303461000073X Published online by Cambridge University Press

differential cross sections then range at a rather low n_b (10^{-33}cm^2) level.

However, when suitably averaged over the many angular degrees of freedom and at higher energy, the total cross-section may well be lifted up at *mb* level. Nuclei disintegration offer a first opportunity to correlated proton stopping (Figs. 5b, 5c), which can be pictured as a charge $Z = 2$, yielding a factor of 4 increase over single proton stopping (Deutsch & Tahir, 1992). Moreover, the π behavior in the given hot and ultradense target may prove highly productive to the hot spot ignition. First, it releases energy through its stopping mechanism. However the most intriguing contribution seems to arise from the various π-catalytic cycles available to DD, TT, and DT nuclear reactions. Its 28 ns lifetime is likely to secure its integrity during the whole compression time available to target.

7. PION CATALYSIS

A typical catalytic cycle is pictured in Figure 6; it straightforwardly highlights the three main advantages of π-catalyzed thermonuclear fusion in a FIS target: (1) The negative pion is already available at $E_b \geq 150$ MeV, while it requires 5–8 GeV in conventional and cold μCF operating in liquid hydrogen at room temperature and $n_{\mathrm{LHD}} = 4.25 \times 10^{22}/\mathrm{cm}^3$ (Nagamine, 2001). (2) The catalytic cycle is trailed a thousand time faster because of the vastly enhanced FIS target density $n_p = 10^{26}\mathrm{cm}^{-3}$ (Breunlich *et al.*, 1989; Jandel *et al.*, 1989; Harley, 1992; Pahlavani & Motevalli, 2009). (3) The density and temperature in highly collisional plasma ($T_p \geq 1$ keV) also secure a catalytic cycle free of the final sticking process of the pion on the resulting alpha particle or other light ions.

Moreover, the given super compressed DT-target offers many opportunities of stable 3-4- or 5-body molecular arrangements able to contribute to the catalytic cycle

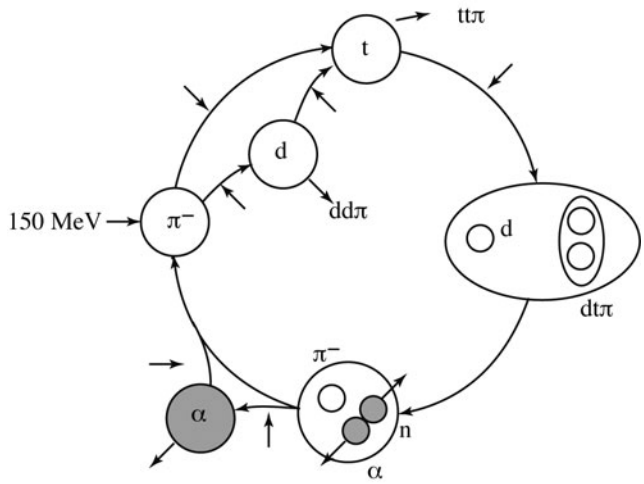

Fig. 6. Pion catalyzed D-T fusion cycle with indications of mains processes (after K. Nagamine, *Hyp. Int.* **138**, 5–13 (2001)).

(Rebane, 2009). 4-body systems such as the $m_1^+m_2^+m_3^-m_4^-$ neutral ones formed by four particles of unit charge, $q_1 = q_2 = 1$, and $q_3 = q_4 = -1$ with masses m_1, m_2, m_3, and m_4 and $m_1^+m_2^+m_3^-$ three-particle ions.

Assuming the mass ordering $m_1 \geq m_2$, $m_3 \geq m_4$, $m_2 \geq m_4$, the lowest dissociation threshold for the four-particle system, E_{th}, in the system of Hartree a.u.($\hbar = 1$, $m_{e=1}, q_e = 1$) is

$$E_{th}(m_1^+m_2^+m_3^-m_4^-) = -\frac{m_1m_3}{2(m_1+m_3)} - \frac{m_2m_4}{2(m_2+m_3)}, \tag{11}$$

while the lowest dissociation (ionization) threshold for the three-particle system is

$$E_{th}(m_1^+m_2^+m_3^-) = -\frac{m_1m_3}{2(m_1+m_4)} \tag{12}$$

It then follows (Rebane, 2009) that combinations $m_1^+m_2^+m_3^-m_4^-$, fulfilling

$$0.4710 \leq \mathrm{s} = \left(\frac{1}{m_1}+\frac{1}{m_3}\right)\Big/\left(\frac{1}{m_2}+\frac{1}{m_4}\right) \leq 2.1231, \tag{13}$$

are obviously stable. This criterion makes it possible to establish stability against dissociation of tens of 4 particles meso molecules, combinations of electrons (e), protons (p), pions (π) deuterons (d), tritons (t), muons (μ) … If the mass of the lightest particle in the system is much smaller than the masses of the other particles, s is outside the interval in Eq. (13). So, the criterion turns inapplicable. See for example, the $t^+d^+p^-e^-$ system (s = 0.0007). More generally, from the stability of the $m_1^+m_2^+m_3^-$ three-particle system, it follows that the $m_1^+m_2^+m_3^-m_4^-$ four-particle system containing an additional particle of mass satisfying the condition $m_4^- \leq m_3^-$ is stable.

In this regard, it is also rather encouraging that the given transitory molecular arrangements can be treated within a Debye approximation. For instance, in an igniting plasma ($n_p \sim 10^{26}$/cc, $T_p \sim$ 3-5 keV) one can witness a persistence of $(\mathrm{MuDT})^+$ molecular ions (Kar & Ho, 2008) with a binding energy ~ 400 eV in a state ($\gamma = 0$, $J = 0$) relative to dπ and tπ atomic structures. Such bound states are equivalent to excited hydrogenic atoms with $n = 12$, and exhibiting anisotropy due to a nearly D^+ or T^+ ion. So, the probability of hadronic π-capture remains very small, in accordance with the strong inequality (a, scattering length)

$$\sigma_{\pi-\mathrm{N}}(\mathrm{a} \sim -0.036\,\mathrm{fm}) << \sigma_{\mathrm{N}-\mathrm{N}}(\mathrm{a} \geq 1.8\,\mathrm{fm}), \tag{14}$$

thus securing an essentially electromagnetic cycling rate (Fig. 6).

Another intriguing effect able to lower by orders of magnitude the tunneling barrier between fusioning nuclei may arise from the frustration experienced by the pion when simultaneously attracted by so density packed D^+ and T^+ nuclei (Kimura & Bonasera, 2004).

https://doi.org/10.1017/S026303461000073X Published online by Cambridge University Press

8. PROVISIONAL CONCLUSIONS

Potential benefits of ICF fast ignition with ultra relativistic electron beams ($\gamma_b \gg 1$), obviously include: (1) Less initial intensity requested. (2) Easier "piercing" through electromagnetic instabilities. (3) Novel stopping mechanism available. (4) Strong Langmuir and EMHD stopping efficient at $\gamma_b \gg 1$. (5) Huge number of possible collisional stopping channels available. Final state interactions seem to offer new prospects to pion-catalyzed fusion with very low production cost, negligible sticking in the very dense and hot FIS plasma, and much faster cycling rate, when contrasted to the usual LHD cold approach. It remains to evaluate potentialities of laser produced proton beams in the 20–40 MeV energy range. Pertaining inelastic hadronic reactions feature differential cross-sections in the *mb* range. So, their investigation in a FIS framework looks highly promising, too.

REFERENCES

Bret, A. & Deutsch, C. (2005). Hierarchy of Beam plasma instabilities up to high densities for fast iginition scenario. *Phys. Plasmas* **12**, 082704.

Breunlich, W.H., Kammel, P., Cohen, J.S. & Leon, M. (1989). Muon-Catalyzed fusion. *Ann. Rev. Nucl. Part. Sci.* **39**, 311–356.

Deutsch, C., Furukawa, H., Mima, K., Murakami, M. & Nishihara, L. (1996). Interaction physics of the fast ignitor concept. *Phys. Rev. Lett.* **77**, 2483–2486.

Deutsch, C., Furukawa, H., Mima, K., Murakami, M. & Nishihara, K. (1997). Interaction physics of the fast ignitor concept. *Laser Part. Beams* **15**, 557–564.

Deutsch, C., Furukawa, H., Mima, K., Murakami, M. & Nishihara, K. (2000). Interaction physics of the ignitor concept, Erratum. *Phys. Rev. Lett.* **85**, 1140–2240.

Deutsch, C. & Tahir, N.A. (1992). Fragmentation and stopping of heavy cluster ions in a lithium target. Application to target implosion. *Phys. Fluids B* **4**, 3735–3746.

Harley, D. (1992). Regeneration and stopping of (alpha-μ)$^+$ on a degenerate plasma. *Phys. Rev. A* **45**, 8981–8983.

Hofstadter, D.R. (1963). *Nuclear and Nucleon Structure*. New York: W.A. Benjamin.

Jandel, M., Froelich, P., Larson, C. & Stodden, C.D. (1989). Reactivation of alpha-mu in muon-catalyzed fusion under plasma conditions. *Phys. Rev. A* **40**, 2799–2802.

Kar, S. & Ho, Y.K. (2008). Bound states and resonance states of the plasma-embedded td mu and dd mu molecular ions. *Eur. Phys. J.D.* **48**, 157–165.

Kimura, S. & Bonasera, A. (2004). Chaos driven fusion enhancement factor at astrophysical energies. *Phys. Rev. Lett.* **93**, 262502.

Kodama, R., Shiraga, H., Shigemori, K., Toyama, Y., Fujioka, S., Azechi, H., Fujiita, H., Habara, H., Hall, T., Izawa, Y., Jitsuno, T., Kitagawa, Y., Krushelnick, K.M., Lancaster, K.L., Mima, K., Nagai, K., Nakai, M., Nishimura, H., Norimatsu, T., Norreys, P.A., Sakabe, S., Tanaka, K.A., Youssef, A. & Zepf, M. (2002). Nuclear fusion - Fast heating scalable to laser fusion ignition. *Nat.* **418**, 933–934.

Malkin, V.M. & Fisch, N.J. (2002). Collective deceleration of relativistic electrons precisely in the core of an inertial-fusion target, *Phys. Rev. Lett.* **89**, 125004.

Myatt, J., Delettrez, J.A., Maximov, A.V., Meyerhofer, D.D., Shory, R.W., Stoeckl, C. & Storm, M. (2009). Optimizing electron-positron pair production on kilojoule-class high-intensity lasers for the purpose of pair-plasma creation. *Phys. Rev. E*, **79**, 066409.

Nagamine, K. (2001). Review of measurements of fusion neutrons in muon catalyzed d-t. *Hyp. Int.* **138**, 5–13.

Pahlavani, M.R. & Motevalli, S.M. (2009). Study of muon catalysed fusion in deuterium-tritium fuel under compressive conditions. *Acta Phys. Pol. B* **40**, 319–329.

Rebane, T.K. (2009). Stability of Coulomb systems. *Phys. At. Nucl.* **72**, 55–58.

Rosenbluth, M. (1950). High energy elastic scattering of electrons on protons high energy elastic scattering of electrons on protons. *Phys. Rev.* **79**, 615–619.

Shearer, J.W., Garrison, J., Wong, J. & Swain, J.E. (1972). Pair production by relativistic electrons from an intense laser focus. *Phys. Rev. A* **8**, 1582–1588.

Starikov, K.V. & Deutsch, C. (2005). Stopping of relativistic electrons in a partially degenerate electron fluid. *Phys. Rev. E* **71**, 026407.

Yabuuchi, T., Das, A., Kumar, G.R., Habaara, H., Kam, P.K., Kodama, R., Mima, K., Norreys, P.A., Sengupta, S. & Tanaka, K.A. (2009). Evidence of anomalous resistivity for hot electron propagation through a dense fustion core in fast ignition experiments. *New J. Phys.* **11**, 09303.

https://doi.org/10.1017/S026303461000073X Published online by Cambridge University Press